^{8}Be scattering potentials from reaction analyses

V. O. Romanyshyn,[1] A. T. Rudchik,[1,*] K. W. Kemper,[2] S. Kliczewski,[3] E. I. Koshchy,[4] O. A. Ponkratenko,[1] K. Rusek,[5] A. Budzanowski,[3] J. Choinski,[6] B. Czech,[3] L. Głowacka,[7] S. Yu. Mezhevych,[1] Val. M. Pirnak,[1] V. A. Plujko,[1] A. A. Rudchik,[1] I. Skwirczyńska,[3] R. Siudak,[3] and A. Szczurek[3]

[1]*Institute for Nuclear Research, Prospect Nauki 47, 03680 Kyiv, Ukraine*

[2]*Physics Department, Florida State University, Tallahassee, Florida 32306-4350, USA*

[3]*H. Niewodniczański Institute of Nuclear Physics, Radzikowskiego 152, PL-31-342 Cracow, Poland*

[4]*Kharkiv National University, Svobody 4, 61077 Kharkiv, Ukraine*

[5]*A. Soltan Institute for Nuclear Studies, Hoża 69, PL-00-681 Warsaw, Poland*

[6]*Heavy Ion Laboratory, Warsaw University, L. Pasteura 5A, PL-02-093 Warsaw, Poland*

[7]*Institute of Applied Physics, Military University of Technology, Kaliskiego 2, PL-00-908 Warsaw, Poland*

(Received 21 October 2008; revised manuscript received 26 March 2009; published 13 May 2009)

New angular distributions for the ^{7}Li(^{10}B, ^{9}Be)^{8}Be reaction at an energy of $E_{\rm lab}(^{10}{\rm B}) = 51$ MeV for the ground and excited states of ^{8}Be were analyzed within the coupled-reaction-channels method. The reactions are dominated by single proton transfer at forward angles except for that to the ^{8}Be 11.35-MeV state, which requires multistep routes for its population. The $^{8}{\rm Be} + {}^{9}{\rm Be}$ potential parameters for ground and excited states of ^{8}Be were deduced by fitting ^{7}Li(^{10}B, ^{9}Be)^{8}Be and ^{10}B(^{7}Li, ^{9}Be)^{8}Be reaction data and are compared with a previously determined $^{7}{\rm Be} + {}^{9}{\rm Be}$ potential. The $^{8}{\rm Be} + {}^{9}{\rm Be}$ real potential is very similar to that for $^{7}{\rm Be} + {}^{9}{\rm Be}$, whereas the imaginary one for $^{8}{\rm Be} + {}^{9}{\rm Be}$ has a much greater spatial extent than that for $^{7}{\rm Be} + {}^{9}{\rm Be}$.

DOI: 10.1103/PhysRevC.79.054609 PACS number(s): 25.70.Hi, 24.10.Eq, 24.10.Ht, 27.20.+n

I. INTRODUCTION

The nucleus ^{8}Be has tremendous future potential for use in reaction spectroscopy [1]. Its being slightly unbound means that most reactions where it appears in the final state will have very different Q values from those that use stable beams, allowing new structures to be probed. For example, reactions such as (^{12}C, ^{8}Be) were proposed [2] as an alternative to (^{6}Li, d) for extracting the α particle structure of nuclei, but the limited detector efficiencies in the 1970s did not allow this alternative to be explored in detail. The recently produced detector arrays that have been built to carry out charged particle reactions induced by radioactive beams have the well-divided substructure and large-angle coverage that allow the detection of ^{8}Be with as great an efficiency as for bound particles, making the original hope for these reactions a reality. However, for these reactions to provide detailed spectroscopic information, knowledge of ^{8}Be optical potentials will be needed, which is the subject of this work.

The present work presents new data for the reaction ^{7}Li(^{10}B, ^{9}Be)^{8}Be taken at the ^{10}B bombarding energy of $E_{\rm lab}(^{10}{\rm B}) = 51$ MeV ($E_{\rm c.m.} = 21$ MeV). These new data are then used in coupled-reaction-channels (CRC) calculations to extract $^{8}{\rm Be} + {}^{9}{\rm Be}$ optical potentials for comparison with previously determined $^{7}{\rm Be} + {}^{9}{\rm Be}$ potentials [3]. To date, the ^{10}B(^{7}Li, ^{9}Be)^{8}Be reaction has been studied only at an energy of $E_{\rm lab}(^{7}{\rm Li}) = 24$ MeV ($E_{\rm c.m.} = 14.12$ MeV) [4] and these data were analyzed within the Hauser-Feshbach statistical model [5].

The CRC method was employed in the present work to interpret the obtained angular distributions. In this scheme optical potentials are needed for both the entrance and exit channels as well as information about the structure of the transferred partners. The entrance-channel $^{7}{\rm Li} + {}^{10}{\rm B}$ optical potential parameters were taken from Ref. [6] and were deduced by fitting elastic scattering data measured simultaneously with the present transfer data. Then, since the shell-model spectroscopic amplitudes for the reaction are known [7], the only piece of missing information, the $^{8}{\rm Be} + {}^{9}{\rm Be}$ optical potential, can be extracted from the reaction analysis.

The paper is organized as follows. In Sec. II, we present the experimental procedure. The results of the CRC analysis of the ^{7}Li(^{10}B, ^{9}Be)^{8}Be and ^{10}B(^{7}Li, ^{9}Be)^{8}Be reaction data and comparison with the previously obtained potential for $^{7}{\rm Be} + {}^{9}{\rm Be}$ are given in Sec. III. Summary and conclusions close our paper.

II. EXPERIMENTAL PROCEDURE

Angular distributions of ^{9}Be from the ^{7}Li(^{10}B, ^{9}Be)^{8}Be reaction together with other ^{7}Li(^{10}B, X) nuclear processes, including $^{10}{\rm B} + {}^{7}{\rm Li}$ scattering [6], were measured at an energy of $E_{\rm lab}(^{10}{\rm B}) = 51$ MeV using a ^{10}B beam from the Warsaw University cyclotron C-200P. The experimental details are given in Ref. [6] and only a brief summary will be presented here. The reaction products were detected by a silicon ΔE-E-telescope and by a telescope with an ionization chamber as the ΔE detector [8].

Part of a typical $\Delta E(E)$ spectrum measured with the silicon ΔE-E detector telescope is presented in Fig. 1. As can be seen, excellent separation of the Be isotopes was achieved in this work.

Typical energy spectra of ^{9}Be from the reactions ^{7}Li(^{10}B, ^{9}Be)^{8}Be are shown in Fig. 2. In Fig. 2(a), the curves show the description of the background from multiparticle

*rudchik@kinr.kiev.ua

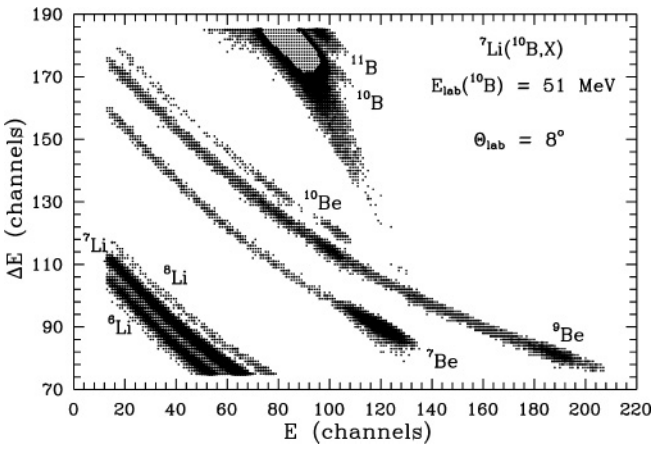

FIG. 1. Typical $\Delta E(E)$ spectrum of the products from ^{7}Li(^{10}B, X) reactions at energy $E_{lab}(^{10}B) = 51$ MeV.

reactions of the ^{7}Li(^{10}B, ^{9}Be)$\alpha\alpha$ type that we model by

$$N(E) = \sum_i N_{0i} \left[1 + \exp\left(-\frac{E - E_1^{(i)} + E_2^{(i)}/2}{h_1^{(i)}}\right)\right]^{-1} \times \left\{1 - \left[1 + \exp\left(-\frac{E - E_1^{(i)} - E_2^{(i)}/2}{h_2^{(i)}}\right)\right]^{-1}\right\}, \quad (1)$$

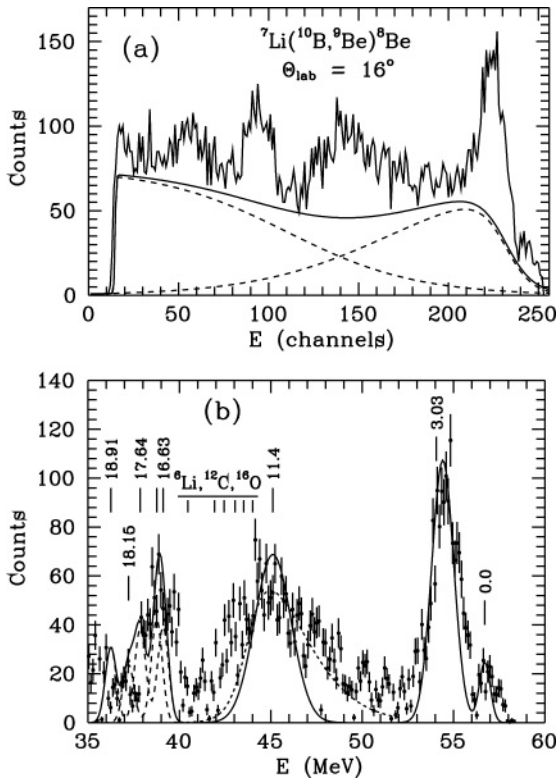

FIG. 2. Typical energy spectra of ^{9}Be from the ^{7}Li(^{10}B, ^{9}Be)^{8}Be reaction at $E_{lab}(^{10}B) = 51$ MeV for the angle $\theta_{lab} = 16^\circ$ (a) with multiparticle reaction background and (b) without. The curves show the calculated background and the Gauss symmetric forms.

with fitting parameters N_{0i}, $E_1^{(i)}$, $E_2^{(i)}$, $h_1^{(i)}$, and $h_2^{(i)}$. The solid curve shows the sum of the individual forms (dashed curves) with the high-energy continuum arising from ^{8}Be $\rightarrow \alpha + \alpha$ and the low-energy one from ^{9}Be. The residual spectrum obtained by subtracting this background is shown in Fig. 2(b). To extract the yields, the peaks were fitted by the sum of Gauss symmetric functions, with the peak positions E_i determined by the corresponding kinetic energies and by fixing the parameters h_i to the width of the elastic-scattering peaks or to the natural level width [curves in Fig. 2(b)]. The broad 3.03- and 11.35-MeV peaks were also fitted by asymmetric forms [Eq. (1); see the dashed curves in Fig. 2(b) for the 11.35-MeV peak] with 1.5- and 3.5-MeV widths, respectively. The difference between the areas under both forms was less than 20% (i.e., likely attributable to the error in background subtraction). The area errors of these peaks were estimated to be 30%. For other peaks the fitting procedure provided areas with errors of about 15%–20%, if the peaks were well resolved, and 30%–40% for poorly resolved peaks.

As one can see in Fig. 2(b), the 11.35-MeV broad peak has microstructure, produced by the (^{10}B, ^{9}Be) reaction products from the ^{6}Li, ^{12}C, and ^{16}O admixture in the ^{7}Li target. Figure 2(b) shows that these reactions can contribute only to the low-energy side of the 11.35-MeV peak. Interest in this state arises because it cannot be populated directly via proton transfer.

The absolute cross sections for the ^{7}Li(^{10}B, ^{9}Be)^{8}Be angular distributions were obtained by multiplying them by the same normalization factor that was determined from the simultaneously measured ^{7}Li + ^{10}B elastic scattering. As shown in Ref. [6], the error in the absolute cross section is 15%.

The resulting angular distributions of the ^{7}Li(^{10}B, ^{9}Be)^{8}Be reaction at $E_{lab}(^{10}B) = 51$ MeV are shown in Figs. 3–7. Owing to the unbound structure of the ^{8}Be ground state, this reaction product was not detected and the reaction angular distributions were measured only at forward angles since ^{9}Be was the detected product.

III. DATA ANALYSIS

A. Calculation procedure

The reaction data were analyzed with the CRC method using optical model potentials in the entrance and exit channels of Woods-Saxon form

$$U(r) = V_0 f(r, R_V, a_V) + i W_S f(r, R_W, a_W) \quad (2)$$

and Coulomb potentials of a uniform charged sphere,

$$V_C(r) = \begin{cases} \dfrac{Z_P Z_T e^2}{2R_C}\left(3 - \dfrac{r^2}{R_C^2}\right), & r \leqslant R_C, \\ \dfrac{Z_P Z_T e^2}{r}, & r > R_C. \end{cases} \quad (3)$$

Here

$$f(r, R_i, a_i) = \left[1 + \exp\left(\frac{r - R_i}{a_i}\right)\right]^{-1}, \quad (4)$$

$$R_i = r_i\left(A_P^{1/3} + A_T^{1/3}\right), \quad i = V, W, C, \quad (5)$$

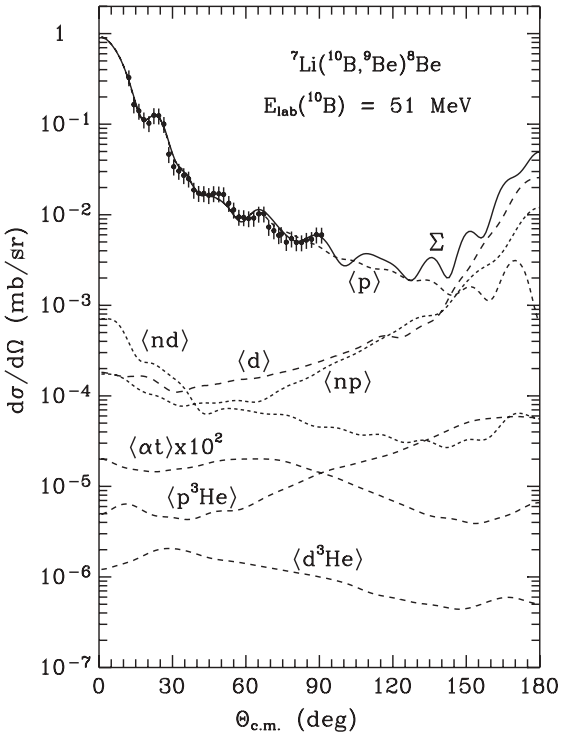

FIG. 3. Angular distribution of the ^{7}Li(^{10}B, ^{9}Be)^{8}Be reaction at $E_{lab}(^{10}B) = 51$ MeV for transitions to the ground states of ^{8}Be and ^{9}Be. The curves show the CRC calculations for different transfers. Curve Σ presents coherent sum of all transfers.

where A_P, A_T and Z_P, Z_T are the mass and charge numbers of ^{7}Li, ^{10}B (entrance channel) and ^{9}Be, ^{8}Be (exit channel).

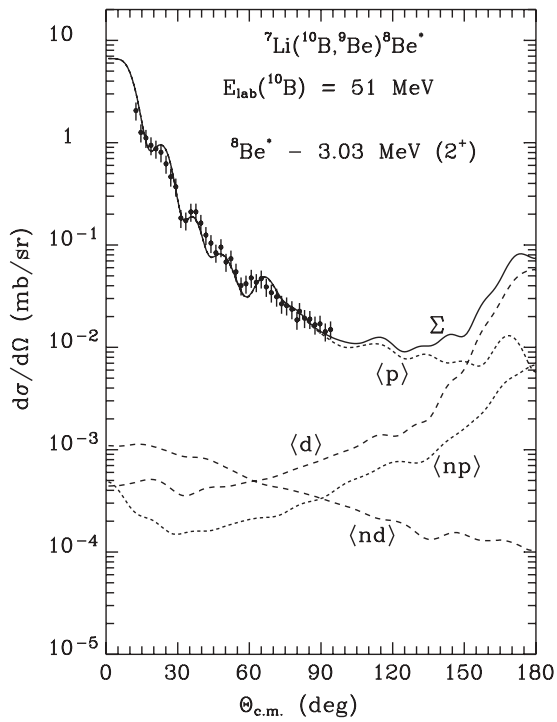

FIG. 4. The same as in Fig. 3 but for the 3.03-MeV (2^{+}) state of ^{8}Be.

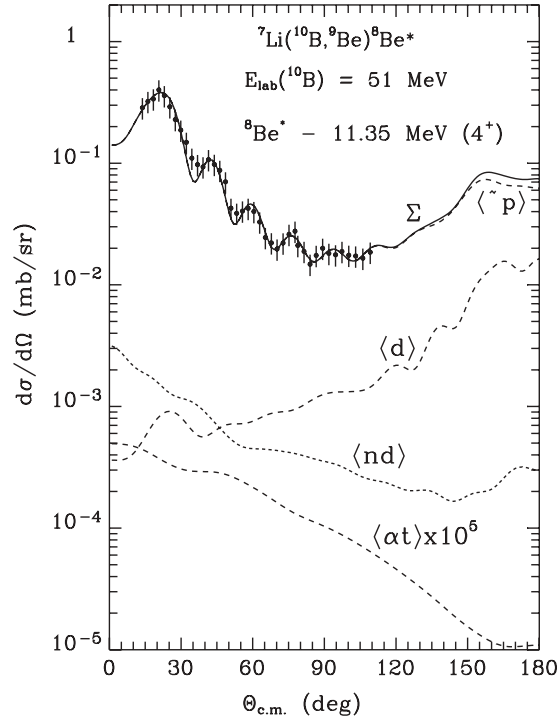

FIG. 5. The same as in Fig. 3 but for the 11.35-MeV (4^{+}) state of ^{8}Be.

The most important transfer reactions as well as ^{7}Li + ^{10}B elastic and inelastic scattering were included in the coupled-channels scheme. The transitions to the excited states of ^{7}Li and ^{10}B were treated as in Ref. [6] (see Fig. 8 there).

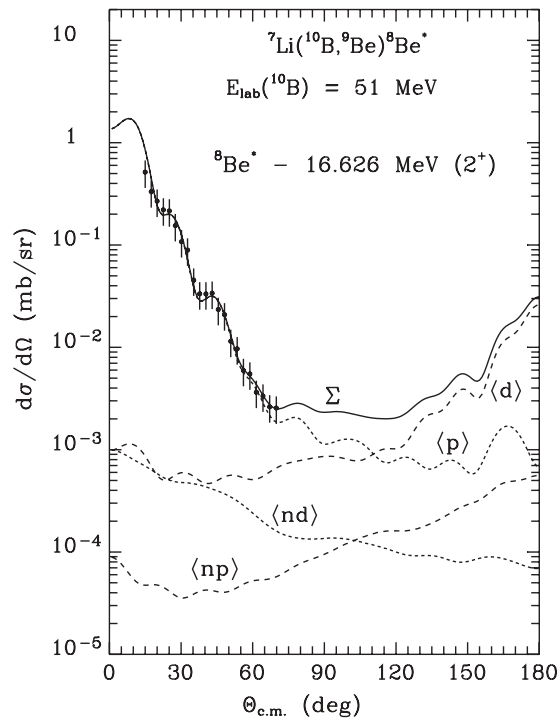

FIG. 6. The same as in Fig. 3 but for the 16.626-MeV (2^{+}) state of ^{8}Be.

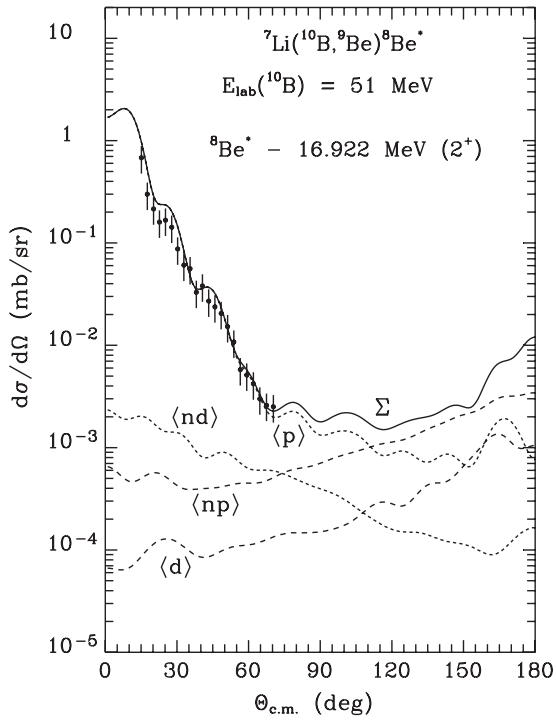

FIG. 7. The same as in Fig. 3 but for the 16.922-MeV (2^+) state of ^{8}Be.

Figure 8 shows the diagrams of one- and two-step transfers, which were included in the calculations.

In the $^7\mathrm{Li} + {}^{10}\mathrm{B}$ entrance channel, the optical potential parameters obtained by fitting the elastic scattering data [6] were used. The $^8\mathrm{Be} + {}^9\mathrm{Be}$ potential was deduced from the experimental data by fitting the exit channel potential parameters

$$X_i = \{V_0, r_V, a_V, W_S, r_W, a_W\} \tag{6}$$

to the reaction data for ground and excited states of ^{8}Be independently while keeping the $^7\mathrm{Li} + {}^{10}\mathrm{B}$ potential parameters and the spectroscopic amplitudes S_x of transferred clusters or nucleons fixed. The parameter $r_C = 1.25$ fm was used in all calculations.

In spite of the fact that the nucleus-nucleus interaction occurs at the nuclear surfaces, the optical potential [Eq. (2)] with only volume absorption was used for both entrance and exit reaction channels, because the penetration barrier for the collision of light nuclei is low and the effective potential surface is close to the center of the interaction of such nuclei. Moreover, the reaction angular distribution is sensitive to the details of the potential surface shape only at the backward angles where the reaction data are absent.

In the fitting procedure, the $^7\mathrm{Li} + {}^{10}\mathrm{B}$ scattering parameters were used as initial ones for the $^8\mathrm{Be} + {}^9\mathrm{Be}$ potential. All parameters [Eq. (6)] were initially adjusted, but we found little sensitivity to the difference between a_V and a_W and so set them equal. The optical potential parameters deduced in the fitting procedure for ground and excited states of ^{8}Be are listed in Table I. The uncertainties of the the deduced parameters of the $^9\mathrm{Be} + {}^8\mathrm{Be}$ potential are about 10%–15%.

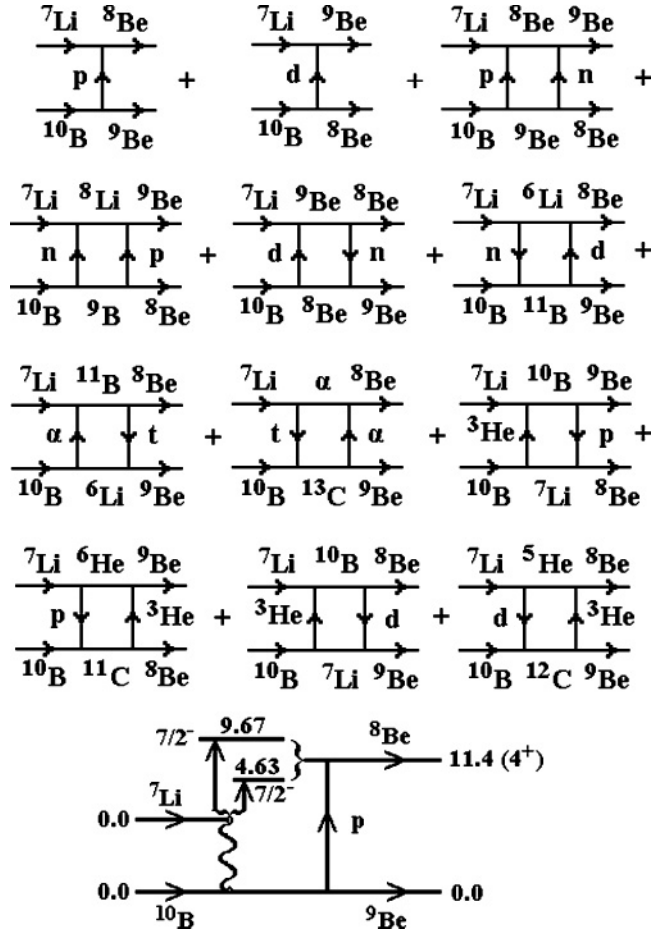

FIG. 8. Diagrams of different mechanisms of the ^{7}Li(^{10}B, ^{9}Be)^{8}Be and ^{7}Li(^{10}B, ^{8}Be)^{9}Be reactions.

The spectroscopic amplitudes S_x of transferred clusters or nucleons x for a nucleus $A = C + x$,

$$S_x = \begin{pmatrix} A \\ x \end{pmatrix}^{1/2} \langle \Psi_A | \Psi_C \Psi_x; \varphi_{Cx} \rangle, \tag{7}$$

were obtained within the translationally invariant shell model (TISM) [7] by using the code DESNA [9,10] and Boyarkina's wave function tables [11]. The calculated values of amplitudes S_x are listed in the Appendix.

The wave function of x for a nucleus $A = C + x$ was calculated by varying the depth of the Woods-Saxon binding potential to reproduce the binding energy of nucleus A. The geometry parameters of the binding potentials were the following: $a = 0.65$ fm and $r_V = 1.25A^{1/3}/(C^{1/3} + x^{1/3})$ fm.

The code FRESCO [12] was used for the CRC calculations. The description of the CRC method used is included in Ref. [12].

B. The ^{7}Li(^{10}B, ^{9}Be)^{8}Be reaction

The measured angular distribution of the ^{7}Li(^{10}B, ^{9}Be)^{8}Be reaction at $E_{\mathrm{lab}}(^{10}\mathrm{B}) = 51$ MeV leading to the ground states of ^{8}Be and ^{9}Be and the results of the corresponding CRC calculations are presented in Fig. 3. The dashed curves labeled

TABLE I. Parameters of the ^{7}Li + ^{10}B and ^{8}Be + ^{9}Be potentials.

$P + T$	$E_{lab}(P)$ (MeV)	$E_{c.m.}$ (MeV)	V_0 (MeV)	r_V (fm)	a_V (fm)	W_S (MeV)	r_W (fm)	a_W (fm)	Ref.
^{7}Li + ^{10}B	24	14.12	150.0	0.790	0.660	11.0	1.250	0.660	[4][a], [6][b]
^{10}B + ^{7}Li	51	21.00	189.9	0.790	0.660	14.5	1.250	0.660	[6][a,b]
^{9}Be + ^{8}Be		24.79	192.4	0.788	0.715	4.0	1.600	0.715	[4][a]
^{9}Be + ^{8}Be		31.67	171.4	0.788	0.760	11.0	1.600	0.760	
^{9}Be + ^{8}Be$^{*}_{3.03}$		21.85	193.4	0.788	0.678	5.0	1.600	0.678	[4][a]
^{9}Be + ^{8}Be$^{*}_{3.03}$		28.73	175.9	0.788	0.760	11.0	1.600	0.760	
^{9}Be + ^{8}Be$^{*}_{11.35}$		13.39	151.2	0.795	0.642	2.0	1.613	0.642	[4][a]
^{9}Be + ^{8}Be$^{*}_{11.35}$		20.27	187.9	0.788	0.660	8.5	1.550	0.660	
^{9}Be + ^{8}Be$^{*}_{16.626}$		15.04	178.3	0.789	0.660	7.0	1.600	0.660	
^{9}Be + ^{8}Be$^{*}_{16.922}$		14.76	178.3	0.789	0.660	7.0	1.600	0.660	

[a]Data.
[b]Potential parameters.

$\langle x \rangle$ show the CRC calculations for the direct transfers of particle x; those labeled $\langle xy \rangle$ present a coherent sum of two-step transfers of particles: first x and then y as well as vice versa. The solid curve Σ shows the coherent sum of all transfers.

At forward angles, the proton transfer (curve $\langle p \rangle$) dominates. The deuteron and $n + p$ plus $p + n$ transfers (curves $\langle d \rangle$ and $\langle np \rangle$) become important at large angles. Other transfers contribute negligibly to this reaction.

The ^{9}Be + ^{8}Be potential parameters were fitted in the CRC calculations. The parameters of this potential deduced at $E_{c.m.} = 14.76$–31.67 MeV (the exit channel for the present study) are listed in Table I.

Clearly, the parameters $a_V = a_W, r_W$, and W_S of this potential differ from that of the ^{7}Li + ^{10}B potential at $E_{c.m.} = 21$ MeV. The angular distribution of the ^{7}Li(^{10}B, ^{9}Be)^{8}Be$^{*}_{3.03}$ reaction at $E_{lab}(^{10}\text{B}) = 51$ MeV for the 3.03-MeV (2^+) state of ^{8}Be is shown in Fig. 4. As in the previous case, proton transfer dominates at forward angles and deuteron transfer is important at backward angles. Sequential particle transfers and inelastic excitation give a small contribution to the calculated cross section of this transition.

Figure 5 shows the measured and calculated angular distribution of the ^{7}Li(^{10}B, ^{9}Be)^{8}Be$^{*}_{11.35}$ reaction at $E_{lab}(^{10}\text{B}) = 51$ MeV for the 11.35-MeV (4^+) state of ^{8}Be. Note that the shape of this angular distribution is very different from that of the other transitions at forward angles. The strength of this transfer is a most surprising result since the shell-model calculation shows that, for the excited system of $^{8}\text{Be}^{*}_{11.35}(4^+) = {}^{7}\text{Li}(3/2^-) + p$, the proton spectroscopic amplitude $S_p = 0$. However, the deuteron- and two-step transfers do not describe the data (see Fig. 5). Therefore, in this case we used the two-step mechanism shown in the diagram placed at the bottom of Fig. 8. First, ^{7}Li is excited to the 4.63-MeV ($7/2^-$) and 9.67-MeV ($7/2^-$) states and then the proton is transferred to form the systems: $^{8}\text{Be}^{*}_{11.35}(4^+) = {}^{7}\text{Li}^{*}_{4.63}(7/2^-) + p$ and $^{8}\text{Be}^{*}_{11.35}(4^+) = {}^{7}\text{Li}^{*}_{9.67}(7/2^-) + p$. For these systems, the proton spectroscopic amplitudes $S_p \neq 0$ (see the Appendix). In Fig. 5, the curve $\langle \tilde{} \text{p} \rangle$ shows CRC calculations for this two-step reaction mechanism. The calculations reproduce very well the experimental data.

Figures 6 and 7 show the measured and calculated angular distributions of the ^{7}Li(^{10}B, ^{9}Be)^{8}Be* reaction at an energy of $E_{lab}(^{10}\text{B}) = 51$ MeV for the transitions to the 16.626-MeV (2^+) and 16.922-MeV (2^+) states of ^{8}Be. For both transitions, direct proton transfer (curves $\langle p \rangle$) dominates at forward angles. At most backward angles, deuteron transfer, with some contribution from sequential $n + p$ transfers, plays an important role.

C. The ^{10}B(^{7}Li, ^{9}Be)^{8}Be reaction

Analysis of the previously reported ^{10}B(^{7}Li, ^{9}Be)^{8}Be data taken at an energy of $E_{c.m.} = 14$ MeV [$E_{lab}(^{7}\text{Li}) = 24$ MeV] [4] adds to information on the energy dependence of the

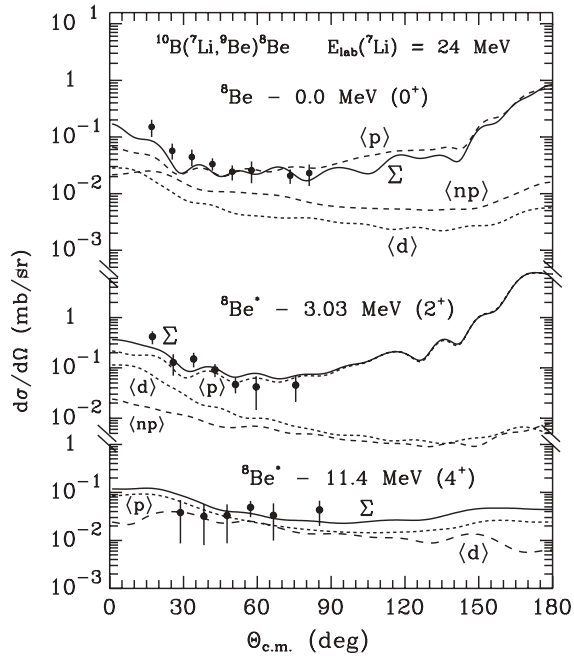

FIG. 9. Angular distribution of the ^{10}B(^{7}Li, ^{9}Be)^{8}Be reaction at $E_{lab}(^{7}\text{Li}) = 24$ MeV [4]. The curves show the CRC calculations for different transfers. Curve Σ presents coherent sum of all transfers.

^{8}Be + ^{9}Be optical potential. Consequently, these data were also included in the CRC analysis.

Figure 9 shows the angular distribution of this reaction, with the curves giving the results of CRC calculations for different transfers. The parameters of the ^{9}Be + ^{8}Be potential deduced from the data fit are listed in Table I. Proton, deuteron, and sequential $n + p$ transfers are important for the transition to the ground state of ^{8}Be at forward angles. In this angular region, the proton and deuteron transfers are important also for the transition to the excited state of ^{8}Be. Curves Σ show the coherent sums of individual transfers. Surprisingly, the data are well reproduced by CRC calculations, without any addition from compound reactions, in contrast to the analysis of Ref. [4].

D. Potential parameters of the ^{8}Be + ^{9}Be scattering system

The parameters of the ^{8}Be + ^{9}Be optical potential [Eq. (6)] deduced by fitting ^{7}Li(^{10}B, ^{9}Be)^{8}Be and ^{10}B(^{7}Li, ^{9}Be)^{8}Be reaction data for different kinetic energies $E_{\text{c.m.}}$ of the ^{9}Be + ^{8}Be system are listed in Table I. All the energies are far above the Coulomb barrier. so the energy dependence of the parameters is very weak, within the error bars. Only the depth of the imaginary potential shows some increase with increasing energy.

In our previous work we have found that the ^{7}Li + ^{9}Be and ^{7}Be + ^{9}Be potentials are in good agreement [3], confirming the general expectation that the scattering of two mirror nuclei that have very similar internal structure should yield very similar scattering potentials. The data used in this comparison were taken from Verma *et al.* [13]. Thus, one can obtain information about the isotopic effect in ^{7}Be and ^{8}Be + ^{9}Be scattering and hence the influence of the internal structure of the scattering partners by comparing the extracted ^{8}Be + ^{9}Be and ^{7}Be + ^{9}Be potentials. Such a comparison is presented in Fig. 10 at the same c.m. energy. The difference between the real parts of the ^{7}Be + ^{9}Be and ^{8}Be + ^{9}Be potentials is small. The main difference is in their imaginary parts, with the ^{8}Be + ^{9}Be potential having a much larger range than that of the ^{7}Be + ^{9}Be potential. This difference means that the flux from the ^{8}Be + ^{9}Be elastic channel is removed at much greater distances between the nuclei than for ^{7}Be scattering and is a consequence of ^{8}Be being unbound.

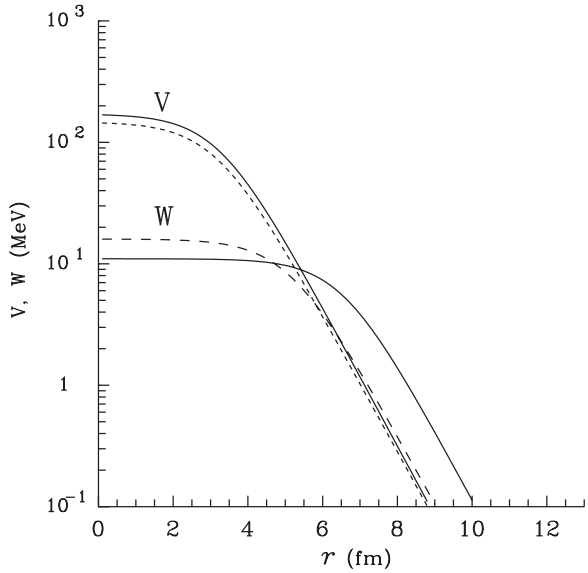

FIG. 10. The ^{8}Be + ^{9}Be potential (solid curves) versus that of ^{7}Be + ^{9}Be (dashed curves) at $E_{\text{c.m.}} = 31.67$ MeV.

IV. SUMMARY AND CONCLUSIONS

Angular distributions of the ^{7}Li(^{10}B, ^{9}Be)^{8}Be reaction leading to the ground and excited states of ^{8}Be were measured at an energy of $E_{\text{lab}}(^{10}\text{B}) = 51$ MeV. The data were analyzed within the coupled-reaction-channels method using optical potentials of Woods-Saxon type for the entrance and exit channels. One- and two-step transfers were included in the coupling scheme as well as the ^{7}Li and ^{10}B excitations. The ^{7}Li + ^{10}B potential parameters obtained by fitting elastic scattering data [6] were employed in the calculations. The ^{8}Be + ^{9}Be potential parameters were deduced by fitting the reaction data. The spectroscopic amplitudes of nucleons and clusters needed for the reaction calculations were obtained within the translationally invariant shell model using the Smirnov-Tchuvil'sky method [7]. The ^{10}B(^{7}Li, ^{9}Be)^{8}Be reaction data at $E_{\text{lab}}(^{7}\text{Li}) = 24$ MeV [4] were also included in the analysis.

The calculations show that, in the ^{7}Li(^{10}B, ^{9}Be)^{8}Be reaction, proton transfer dominates at forward angles whereas a sum of proton, deuteron, and sequential $n + p$ transfers are important at backward angles. Similar mechanisms are also observed for the lower energy in the ^{10}B(^{7}Li, ^{9}Be)^{8}Be reaction. The nonzero cross section for transfer to the ^{8}Be 11.35-MeV state requires large contributions from multistep processes for its population.

The ^{8}Be + ^{9}Be potential parameters were compared to ^{7}Be + ^{9}Be potential ones. The real potentials are remarkably similar for the two systems but the dependence in the imaginary ones demonstrates their marked dependence on the internal structures of the two systems. It is hoped that the derived ^{8}Be potentials found in this and previous works can be exploited in reactions such as (^{12}C, ^{8}Be), where the positive Q value of this reaction, when compared to traditional α transfer reactions such as (^{6}Li, d), can be used to study α clustering in nuclei at high excitation energies. Modern silicon-detector arrays will make it possible to measure reactions with the unbound product ^{8}Be in the exit channel as efficiently as that for bound particles and can be a very rich area for future study.

ACKNOWLEDGMENTS

We thank Prof. A. Sobiczewski and Prof. J. Jastrzebski for their interest in this work. One of us (KWK) acknowledges support of the state of Florida in this work.

APPENDIX

TABLE II. Spectroscopic amplitudes S_x of the particles x in $A = C + x$ systems.

A	C	x	nL_j	S_x	A	C	x	nL_j	S_x
^{7}Li	^{4}He	t	$2P_{3/2}$	−1.091	^{9}B	^{8}Be	p	$1P_{3/2}$	0.866
^{7}Li	^{5}He	d	$2S_1$	−0.674[a]	^{9}B	^{8}Be$^*_{2.94}$	p	$1P_{1/2}$	−0.573[a]
			$1D_1$	−0.121[a]				$1P_{3/2}$	0.573
			$1D_3$	0.676[a]	^{9}B	^{8}Be$^*_{16.63}$	p	$1P_{1/2}$	−0.265[a]
^{7}Li	^{6}He	p	$1P_{3/2}$	0.805	9B	^{8}Be$^*_{16.92}$	p	$1P_{1/2}$	0.484[a]
^{7}Li	^{6}Li	n	$1P_{1/2}$	−0.657				$1P_{3/2}$	0.968
			$1P_{3/2}$	−0.735[a]	^{10}B	^{6}Li	α	$2D_2$	−0.125
^{8}Li	^{7}Li	n	$1P_{1/2}$	0.478	^{10}B	^{7}Li	^{3}He	$2P_{3/2}$	0.419
^{8}Be	^{4}He	α	$3S_0$	1.225				$1F_{5/2}$	−0.104[a]
^{8}Be	^{5}He	^{3}He	$2P_{3/2}$	−1.102[a]				$1F_{7/2}$	−0.347
^{8}Be	^{6}Li	d	$2S_1$	1.217	^{10}B	^{8}Be	d	$1D_3$	0.811
^{8}Be$^*_{2.94}$	^{6}Li	d	$1D_1$	0.455	^{10}B	^{8}Be$^*_{2.94}$	d	$2S_1$	−0.130
			$1D_2$	−0.588[a]				$1D_1$	0.200
			$1D_3$	0.696				$1D_2$	−0.633[a]
^{8}Be$^*_{11.4}$	^{6}Li	d	$1D_3$	0.544				$1D_3$	0.981
^{8}Be$^*_{16.63}$	^{6}Li	d	$1D_1$	−0.633	^{10}B	^{8}Be$^*_{11.4}$	d	$1D_1$	0.475
			$1D_2$	−0.272[a]				$1D_2$	−0.457[a]
			$1D_3$	0.644				$1D_3$	0.303
^{8}Be$^*_{16.92}$	^{6}Li	d	$2S_1$	−1.089	^{10}B	^{8}Be$^*_{16.63}$	d	$2S_1$	0.475
^{8}Be	^{7}Li	p	$1P_{3/2}$	1.234[a]				$1D_1$	0.198
^{8}Be$^*_{2.94}$	^{7}Li	p	$1P_{1/2}$	−0.730				$1D_2$	−0.376[a]
			$1P_{3/2}$	−0.730[a]	^{10}B	^{8}Be$^*_{16.92}$	d	$1D_1$	−0.219
^{8}Be$^*_{11.4}$	^{7}Li$^*_{4.63}$	p	$1P_{1/2}$	−0.873				$1D_2$	0.231[a]
			$1P_{3/2}$	−0.738[a]				$1D_3$	0.179
^{8}Be$^*_{11.4}$	^{7}Li$^*_{9.67}$	p	$1P_{1/2}$	−0.873	^{10}B	^{9}Be	p	$1P_{3/2}$	1.185
			$1P_{3/2}$	−0.738[a]	^{10}B	^{9}B	n	$1P_{3/2}$	−1.185
^{8}Be$^*_{16.63}$	^{7}Li	p	$1P_{1/2}$	0.338	^{11}B	^{7}Li	α	$3S_0$	−0.638
^{8}Be$^*_{16.92}$	^{7}Li	p	$1P_{1/2}$	0.390				$2D_2$	−0.422
			$1P_{3/2}$	−0.781[a]	^{11}B	^{8}Be	t	$2P_{3/2}$	0.641
^{9}Be	^{6}He	^{3}He	$2P_{3/2}$	−0.236	^{11}B	^{8}Be$^*_{11.4}$	t	$1F_{5/2}$	0.578[a]
^{9}Be	^{6}Li	t	$1P_{1/2}$	−0.192				$1F_{7/2}$	−0.431
			$1P_{3/2}$	−0.215[a]	^{11}B	^{9}Be	d	$2S_1$	−0.607[a]
^{9}Be	^{7}Li	d	$2S_1$	−0.226[a]				$1D_1$	−0.109[a]
			$1D_1$	0.111[a]				$1D_3$	0.610
			$1D_3$	−0.624[a]	^{11}B	^{10}B	n	$1P_{3/2}$	−1.347[a]
^{9}Be	^{8}Li	p	$1P_{1/2}$	−0.375[a]	^{11}C	^{8}Be	^{3}He	$2P_{3/2}$	0.641
^{9}Be	^{8}Be	n	$1P_{3/2}$	0.866	^{11}C	^{10}B	p	$1P_{3/2}$	−1.347[a]
^{9}Be	^{8}Be$^*_{2.94}$	n	$1P_{1/2}$	−0.573[a]	^{12}C	^{9}Be	^{3}He	$2P_{3/2}$	1.224[a]
			$1P_{3/2}$	0.573	^{12}C	^{10}B	d	$1D_3$	1.780
^{9}Be	^{8}Be$^*_{16.63}$	n	$1P_{1/2}$	−0.265[a]	^{13}C	^{9}Be	α	$2D_2$	0.504[a]
^{9}Be	^{8}Be$^*_{16.92}$	n	$1P_{1/2}$	0.484[a]	^{13}C	^{10}B	t	$1F_{5/2}$	0.108[a]
			$1P_{3/2}$	0.968				$1F_{7/2}$	0.747

[a] $S_{\text{FRESCO}} = (-1)^{J_C+j-J_A} S_x = -S_x$.

[1] D. Robson, Nucl. Phys. **A204**, 523 (1973).
[2] G. R. Morgan and N. R. Fletcher, Phys. Rev. C **16**, 167 (1977).
[3] A. T. Rudchik *et al.*, Nucl. Phys. At. Energ. **3**, 45 (2008).
[4] W. Kohler *et al.*, Nucl. Phys. **A290**, 233 (1977).
[5] W. Hauser and H. Feshbach, Phys. Rev. **87**, 366 (1952).
[6] A. T. Rudchik *et al.*, Eur. Phys. J. A **33**, 317 (2007).
[7] Yu. F. Smirnov and Yu. M. Tchuvil'sky, Phys. Rev. C **15**, 84 (1977).
[8] V. K. Chernievsky *et al.*, Sci. Pap. Inst. Nucl. Res. **2**, 216 (2002).
[9] A. T. Rudchik and Yu. M. Tchuvil'sky, Computer code DESNA, Report KIYAI-82-12, Institute for Nuclear Research, Ukrainian Academy of Science, Kyiv, 1982.
[10] A. T. Rudchik and Yu. M. Tchuvil'sky, Ukr. Phys. J. **30**, 819 (1985).
[11] A. N. Boyarkina, Structure of $1p$-shell Nuclei, Moscow State University report, 1973.
[12] I. J. Thompson, Comput. Phys. Rep. **7**, 167 (1988).
[13] S. Verma *et al.*, Eur. Phys. J. Spec. Topics **150**, 75 (2007).